

High-spatial-resolution OFDR with single interferometer using self-compensation method

Huajian Zhong^{a,b}, Cailing Fu^{a,b,*}, Lijie Wang^c, Bin Du^{a,b}, Pengfei Li^{a,b}, Yanjie Meng^{a,b},
Lin Chen^{a,b}, Chao Du^{a,b}, Yiping Wang^{a,b}

^a Key Laboratory of Optoelectronic Devices and Systems of Ministry of Education and Guangdong Province, College of Physics and Optoelectronic Engineering, Shenzhen University, Shenzhen 518060, China

^b Shenzhen Key Laboratory of Photonic Devices and Sensing Systems for Internet of Things, Guangdong and Hong Kong Joint Research Centre for Optical Fibre Sensors, Shenzhen University, Shenzhen 518060, China

^c Chongqing University of Technology, Chongqing 400000, China

ARTICLE INFO

Keywords:

Optical frequency domain reflectometry
Distributed optical fiber sensing
Phase noise

ABSTRACT

A high-spatial-resolution optical frequency domain reflectometry (OFDR) with single interferometer was proposed by using self-compensation method (SCM). The auxiliary interferometer (AI) of conventional OFDR was replaced by a processed arc end of the fiber under test (FUT) to generate a reflection signal with appropriate intensity. The actual instantaneous optical frequency (IOF) was successfully extracted from the arc end of the FUT. Combining the arc end and SCM, the phase noise of the proposed OFDR was successfully eliminated to obtain the compensated signal with high signal-to-noise ratio (SNR). Moreover, the influence of delay fiber (DF) length on the compensation effect was theoretically and experimentally analyzed. The proposed OFDR achieved the distributed temperature sensing with a high-spatial-resolution of 3 mm without sacrificing measurement performance, where the measured distance of the FUT was ~ 108 m. The high-spatial-resolution of 5 mm was still achieved when the measured distance of the FUT was increased to ~ 170 m. Such an OFDR system with low cost and good performance has development potential in the field of distributed measurement.

1. Introduction

Distributed optical fiber sensing based on optical frequency domain reflectometry (OFDR) [1] and optical time domain reflectometry (OTDR) [2] could realize distributed multi-parameter measurement along the fiber under test (FUT) chain. The sensing distance of OTDR is tens or even hundreds of kilometers, but its spatial resolution is limited to meter-level due to the optical pulse width [3,4]. Compared with OTDR, a high spatial resolution of OFDR in millimeter-level depends on the sweep range of tunable laser source (TLS) [5–7]. OFDR has been widely used in distributed temperature [8,9], strain/shape [10–12], and liquid refractive index [13] measurement. However, the deterioration of the spatial resolution induced by nonlinearity of TLS is the main challenge in OFDR. Various schemes based on hardware or algorithms have been proposed to solve it. For example, the scheme based on hardware was presented, i.e., using an auxiliary interferometer (AI) to provide external clock to realize equal frequency interval sampling [6,7,10–15], but the measurable distance of FUT was limited by the length of the delay fiber in AI. Meanwhile, an algorithm of auxiliary compensation

method (ACM) was also proposed [16], i.e., using the obtained instantaneous optical frequency (IOF) of the TLS based on AI to interpolate the main interferometer signal to realize compensation, but it was time-consuming. Among them, the introduction of AI not only complicates the structure, but also requires higher acquisition equipment. To optimize or simplify the OFDR, a flexible and compact OFDR was demonstrated, which combined all functions without increasing complexity and cost [17]. In addition, an auxiliary reflection peak generated by connectors in FUT was used to compensate the phase deviation [18]. Besides, an OFDR integrating AI into main interferometer was also proposed to realize the acquisition and compensation of single channel signal [19]. However, the Rayleigh backscattering of the main interferometer would be interfered by the high-intensity signal of AI, and setting the auxiliary peak inside the FUT would also affect the compensation effect under long distance [20], resulting in the deterioration of the spatial resolution. In addition, most of the previously reported OFDR based on commercial TLS showed a measurement distance of only tens of meters.

In this letter, a high-spatial-resolution OFDR with single interferometer was proposed by using self-compensation method (SCM) to eliminate

* Corresponding author at: Key Laboratory of Optoelectronic Devices and Systems of Ministry of Education and Guangdong Province, College of Physics and Optoelectronic Engineering, Shenzhen University, Shenzhen 518060, China.

E-mail address: fucailing@szu.edu.cn (C. Fu).

<https://doi.org/10.1016/j.optlaseng.2022.107341>

Received 23 August 2022; Received in revised form 29 September 2022; Accepted 17 October 2022

Available online 23 October 2022

0143-8166/© 2022 Elsevier Ltd. All rights reserved.

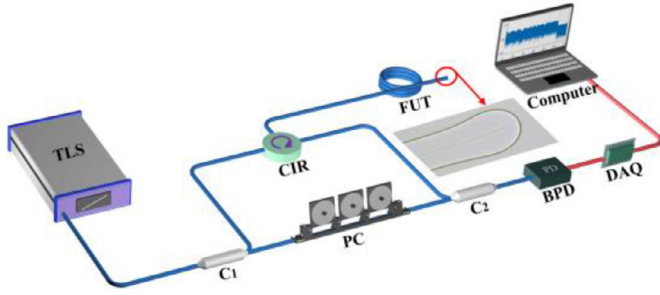


Fig. 1. Schematic diagram of the OFDR with single interferometer. TLS: tunable laser source; C: coupler; CIR: circulator; PC: polarization controller; FUT: fiber under test; BPD: balanced photo-detector; DAQ: data acquisition card. Inset: micrograph of the arc end of FUT.

the phase noise. The auxiliary interferometer (AI) was replaced by an arc end of fiber under test (FUT) to generate a reflection signal with appropriate intensity. The accuracy of the actual instantaneous optical frequency (IOF) extracted by auxiliary compensation method (ACM) based on AI in conventional OFDR, and the SCM based on the arc end of FUT in the proposed OFDR, was investigated and compared. Moreover, the influence of delay fiber (DF) length on the compensation effect was theoretically and experimentally analyzed. Subsequently, the temperature sensing performance of the proposed OFDR with single interferometer and conventional OFDR with AI was also compared. Furthermore, the spatial resolution was further investigated when the length of FUT was increased to ~ 170 m.

2. Experimental setup and methods

As shown in Fig. 1, an OFDR with single interferometer was built and demonstrated. The output of a tunable laser source (TLS) was split into two beams, i.e., reference and probe lights, via a coupler (C_1). The beat signal generated by interference between the reference and probe lights was converted into electrical signal using a balanced photo-detector (BPD), and then collected by a data acquisition card (DAQ), where the sampling rate was 40 MHz/s. In the conventional OFDR, an AI was used for frequency sampling [14] or resampling [16] to eliminate the phase noise induced by the nonlinearity of the TLS. As we know, the existence of phase noise would broaden the beat signal of FUT in the distance domain, resulting in the deterioration of the spatial resolution. Compared with the conventional OFDR, the AI in the proposed OFDR was replaced by an arc end of FUT to generate a reflection signal with appropriate intensity to compensate the beat signal, as shown in the inset in Fig. 1. Note that the detailed fabrication process of the arc end was listed as follows. The FUT with the cleaved end was placed on a fiber holder in a commercial fusion splicer (FSM-60S), then the end face was heated by electrical arc discharge to shape the end into an arc. Another end of the FUT was connected to the proposed OFDR, which was used to measure the reflection intensity and signal-to-noise ratio (SNR) during the heating process. In this way, the self-compensation method (SCM) was adopted to eliminate the phase noise in the proposed OFDR with single interferometer, corresponding to the auxiliary compensation method (ACM) in conventional OFDR.

The detailed process to eliminate the phase noise with the SCM is illustrated in Fig. 2, labeled by gray border. Firstly, the beat signal, i.e., measurement or reference signal, of the whole FUT was acquired by the DAQ. Secondly, a band-pass filter [14], was employed to extract the beat signal obtained by the interference between the local light and reflection signal at the arc end from the afore-obtained beat signal. Ideally, the linear IOF, i.e., v , of the TLS in one cycle could be given by [16,21].

$$v(t) = v_0 + \gamma t, \quad (1)$$

where v_0 and γ are the initial optical frequency and sweep rate of the TLS, respectively. The instantaneous phase of the TLS, i.e., $\varphi(t)$, could

be obtained by integrating Eq. (1) and given by

$$\varphi(t) = 2\pi \int_0^t v(t)dt + \varphi_0 = 2\pi v_0 t + \pi \gamma t^2 + \varphi_0, \quad (2)$$

where φ_0 is the initial phase. Considering a phase noise term, i.e., $\theta(t) - \theta(t - \tau_z)$, and ignoring the direct-current and phase constant terms, the beat signal obtained by the interference between the local light and reflection signal at the arc end of the FUT could be given by

$$U(t) = \left| E_0 \exp[j\varphi(t)] + \sqrt{R} E_0 \exp[j\varphi(t - \tau_z)] \right|^2 \\ = 2\sqrt{R} E_0^2 \cos[2\pi \gamma \tau_z t + \theta(t) - \theta(t - \tau_z)], \quad (3)$$

where E_0 and j are the amplitude of the optical electric field and imaginary unit, R_z and τ_z are the reflectivity and the delay time at the arc end of the FUT, respectively. Thirdly, the actual IOF, i.e., v_1 , could be accurately extracted by performing the Hilbert transform, i.e. $H[U(t)]$, on Eq. (3) and taking the arctangent function. Then the actual IOF could be given by

$$v_1(t) = \arctan \left\{ \frac{H[U(t)]}{U(t)} \right\} / (2\pi \tau_z). \quad (4)$$

Note that the actual IOF, i.e., v_1 , was not completely linear due to the phase noise term, i.e., $\theta(t) - \theta(t - \tau_z)$. Finally, the actual IOF was rearranged into linear IOF, which was used for cubic interpolation of the beat signal, so as to eliminate the phase noise and obtain compensated measurement or reference signal. Therefore, the premise of successfully eliminating the phase noise to achieve signal compensation was that the actual IOF could be accurately obtained.

As shown in Fig. 2, the sensing demodulation process based on the SCM was divided into four steps. Step 1: the compensated measurement and reference signals were transformed into distance domain by fast Fourier transform (FFT). Step 2: the sensing region was selected in the afore-obtained distance domain using a sliding window with N sampling points, and transformed into the optical frequency domain using inverse fast Fourier transform (IFFT), i.e., obtaining measurement and reference spectra. Step 3: the cross-correlation operation between measurement and reference spectra were conducted. Step 4: the spectral shift of the sensing region for the FUT could be obtained by repeating Steps 2 and 3 for m times.

The theoretical spatial resolution, i.e., Δz , of OFDR could be given by [5]

$$\Delta z = c/2n\Delta v, \quad (5)$$

where c is the velocity of light in a vacuum, n is the refractive index of the medium, and Δv is the sweep range of the TLS. Considering a sliding window with N sampling points, the sensing spatial resolution, i.e., Δl , could be given by

$$\Delta l = N\Delta z. \quad (6)$$

3. Experimental results and discussions

To verify the feasibility of the SCM based on an arc end of the FUT, the accuracy of extracted actual IOF, i.e., v_1 , was firstly investigated. In the experiment, the sweep range, i.e., Δv , and the sweep rate, i.e., γ , were set to 10 nm (1250 GHz) and 80 nm/s (10,000 GHz/s). The obtained beat signal and distance domain along the FUT are illustrated in Fig. 3(a) and (b). As shown in the enlarged view of Fig. 3(a), the beat signal was composed of Rayleigh backscattering and reflection signals along the FUT, where the frequency components were different. Then a band-pass filter was applied to extract the beat signal obtained by the interference between the local light and reflection signal at the arc end, as shown in Fig. 3(c). Thus, the actual IOF could be extracted from Fig. 3(c) using Eq. (4). As shown in Fig. 3(d), the sweep rate and range calculated by linear fit were 10,001.525 GHz/s (80.013 nm/s), 1250.025 GHz (10.0002 nm), respectively, which was close to the corresponding set parameters of the TLS, i.e., 10 nm and 80 nm/s. Unfortunately, it was obviously that the scanning of commercial TLS was not

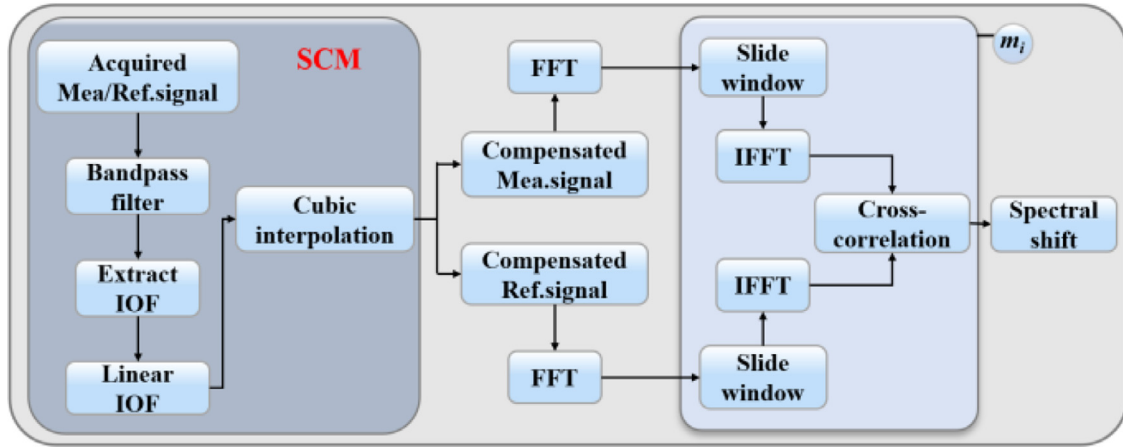


Fig. 2. Flow chart for demodulating using the self-compensation method (SCM) based on the proposed OFDR, where the SCM was used to obtain the compensated measurement and reference signals, respectively. m_i represents the number of processing times. IOF: instantaneous optical frequency; Mea. signal: measurement signal; Ref. signal: reference signal. FFT: fast Fourier transform; IFFT: inverse fast Fourier transform.

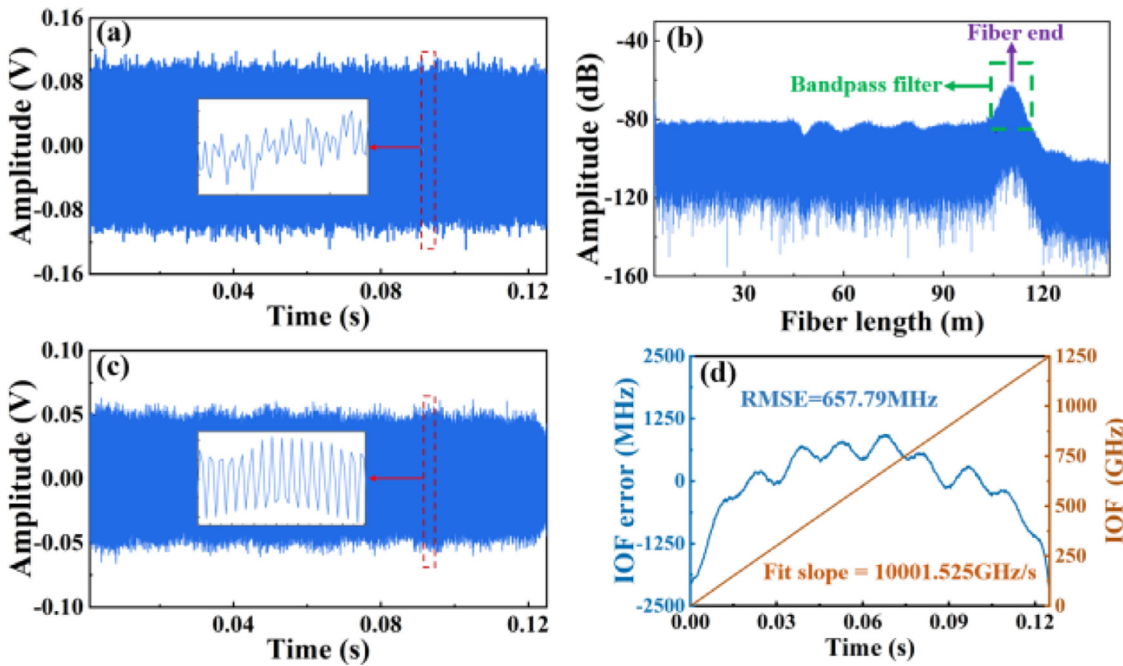


Fig. 3. (a) Beat signal and (b) distance domain of the FUT; (c) beat signal obtained by using a band-pass filter for FUT arc end in Fig. (b); (d) actual instantaneous optical frequency (IOF) obtained from Fig. (c) using Eq. (4). Insets of Fig. (a) and (c): enlarged views of beat signal before and after bandpass filtering.

completely linear, but exhibited a large frequency error, especially in the beginning and end stages. The calculated root mean square error (RMES) was 657.79 MHz, which was mainly caused by the nonlinearity of the TLS and uncontrollable experimental errors.

To further illustrate that the proposed arc end could replace the AI, the accuracy of actual IOF, i.e., v_1 , obtained by using the SCM with single interferometer and ACM with AI were compared and investigated. To make the experimental results reliable, a coupler (1×2) was added between the TLS and C_1 in Fig. 1. Then the output of the TLS was divided into two parts. One part entered into the AI, and the other part entered into the proposed OFDR, i.e., single interferometer shown in Fig. 1. Note that the same BPD and delay fiber (DF) with same length were used, and beat signals were synchronously collected by the DAQ. Under the same sweep range, i.e., 10 nm, four groups of sweep rates, i.e., 50, 80, 150, and 160 nm/s, respectively, were investigated. As shown

in Fig. 4(a), the IOF curves obtained by the OFDR with AI and single interferometer were almost completely coincide, where the corresponding linear fitting slopes were 49.995, 80.016, 149.896, 159.867 nm/s and 49.994, 80.014, 149.895, 159.873 nm/s, respectively. Taking the IOF obtained by OFDR with AI and single interferometer as the theory value and measured value, the relative error of IOF could be calculated by

$$\text{Relative error} = \frac{|\text{Measured value} - \text{Theory value}|}{\text{Theory value}} \times 100\%. \quad (7)$$

Note that the relative error could not be calculated when the theory value was equal to zero. As shown in Fig. 4(b), the relative errors of IOF were relatively tiny, i.e., within 0.006%, at different sweep rates, which indicated that the proposed OFDR with single interferometer using an arc end of the FUT instead of the AI could also accurately extract the

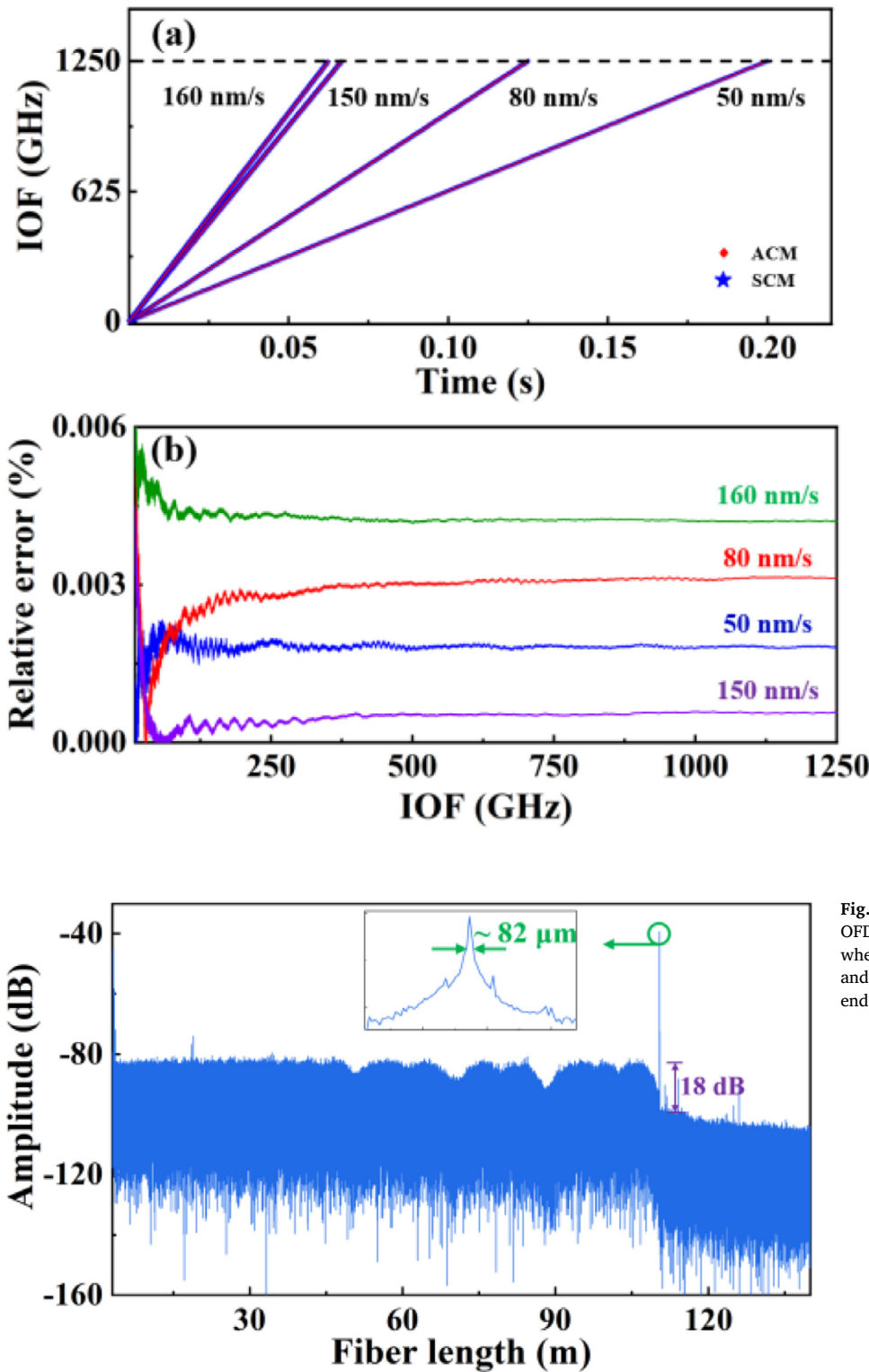


Fig. 4. (a) The actual IOFs obtained by using the ACM and SCM based on OFDR with AI and single interferometer, when the sweep range of the TLS was 10 nm and the sweep rates were 50, 80, 150 and 160 nm/s, respectively; (b) the relative errors of IOF obtained by using the SCM relative to the ACM.

Fig. 5. Compensated distance domain of FUT in the OFDR with single interferometer by using the SCM, where the 3-dB spatial resolution and SNR was 82 μm and 18 dB, respectively. Inset: enlarged view of fiber end reflection peak.

IOF of the TLS based on the proposed SCM. Therefore, the beat signal could be compensated by using the proposed system and SCM, so as to eliminate the phase noise.

Moreover, the compensated distance domain of FUT with a length of more than 100 m obtained by the SCM is illustrated in Fig. 5. As shown in the enlarged view of Fig. 5, the 3-dB spatial resolution at the reflection peak was ~82 μm, which was equal to the theoretical value calculated by Eq. 5 ($\Delta\nu = 10$ nm), i.e., 82 μm. As shown in Fig. 5, the

reflection intensity of ~-40 dB and the SNR of ~18 dB were observed. Note that the higher the SNR, the better the obtained arc end quality. Consequently, a processed arc end of FUT in the proposed OFDR with single interferometer could be employed to generate a reflection signal to successfully extract the IOF, and finally achieved good compensation effect.

When the actual IOF was used to interpolate compensate signal, the influence of DF length on the compensation effect was also analyzed.

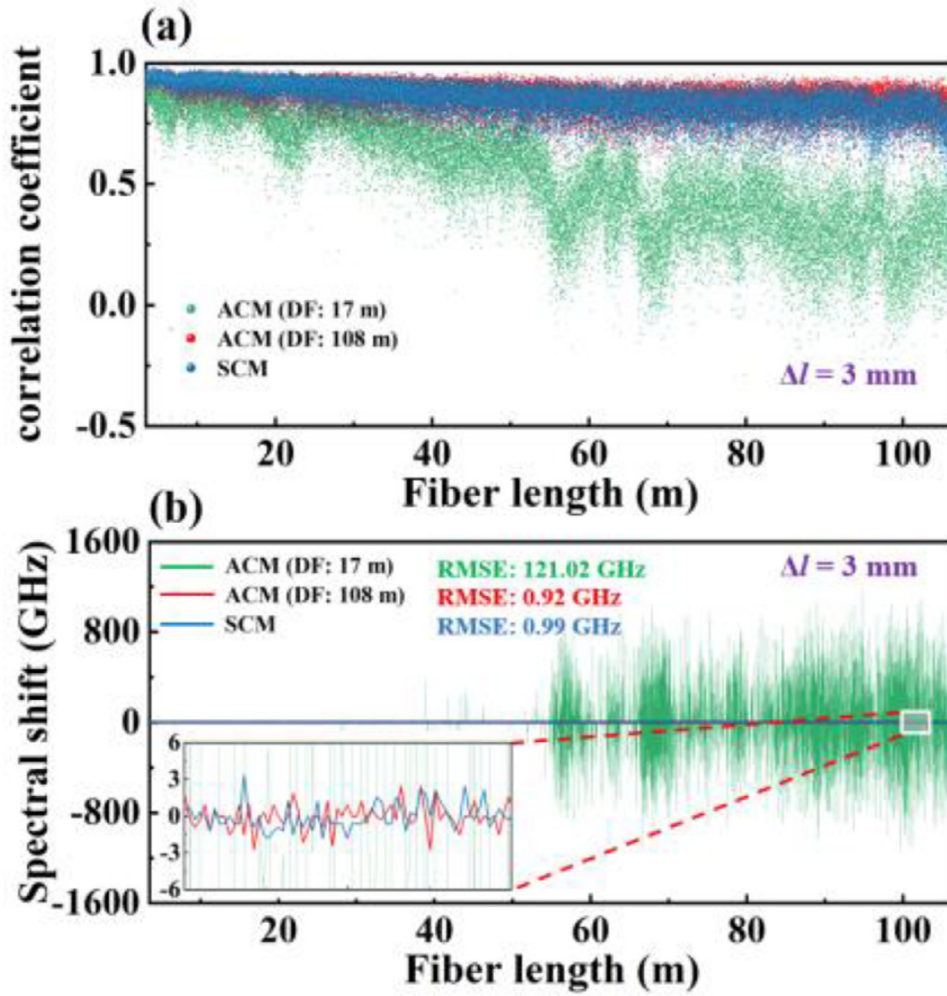


Fig. 6. (a) Cross-correlation coefficients and (b) spectral shifts obtained by using the ACM with ~17 m and ~108 m long DF, and SCM with the arc end, respectively, when no temperature change was applied to the 108 m long FUT, labeled by green, red and blue dot and curves, respectively. Insets: enlarged view of the spectral shift. Note that the spatial resolution, i.e., Δl , was 3 mm.

The beat signal obtained by the interference between the local light and the backscattered light along the FUT could be given by

$$U_{FUT}(t) = \sum_{i=1}^L 2\sqrt{R_i}E_0^2 \cos [2\pi\gamma\tau_i t + \theta(t) - \theta(t - \tau_i)], \quad (8)$$

where L is the number of scatters along the FUT, R_i and τ_i are the reflectivity and the delay time of the backscatters, respectively. As can be seen from Eq. (8), the term of $\theta(t)$ in the phase noise term is independent of the delay time, i.e., independent of the FUT length, while the term of $\theta(t - \tau_i)$ is dependent on the FUT length. Therefore, the phase noise in the beat signal, i.e., $\theta(t) - \theta(t - \tau_i)$, would gradually increase with the increase of the FUT length, resulting in the sharp deterioration of spatial resolution. According to Eq. (3), the actual IOF of the beat signal with a delay time of τ_z contained a phase noise term, i.e., $\theta(t) - \theta(t - \tau_z)$. When the delay time of the DF is much smaller than that of the backscatters of the FUT, i.e., $\tau_z \ll \tau_i$, corresponding to $\theta(t) - \theta(t - \tau_z) \ll \theta(t) - \theta(t - \tau_i)$, the actual IOF extracted from DF could not eliminate all phase noise along the FUT after being used to interpolate the U_{FUT} . On the contrast, when the delay time of the DF is much greater than that of the backscatters of the FUT, i.e., $\tau_z \geq \tau_i$, corresponding to $\theta(t) - \theta(t - \tau_z) \geq \theta(t) - \theta(t - \tau_i)$, the actual IOF extracted from DF could be used to eliminate all phase noise along the FUT. For the proposed OFDR with single interferometer, the beat signal based on Eq. (3) obtained from the arc end of FUT always met the above condition, i.e., $\theta(t) - \theta(t - \tau_z) \geq \theta(t) - \theta(t - \tau_i)$.

To verify the above analysis, an experiment was performed. In the experiment, the sweep rate and range of the TLS were set to 80 nm/s and 10 nm, respectively, and the length of FUT was 108 m. To better evaluate the quality and reliability of the compensated signal, the cross-correlation coefficient, i.e., ρ , was employed to calculate the similarity between the compensated measurement signal (U_{Mea}) and reference signal (U_{Ref}):

$$\rho(U_{Mea}, U_{Ref}) = \frac{\text{cov}(U_{Mea}, U_{Ref})}{(\text{var}[U_{Mea}] \text{var}[U_{Ref}])^{\frac{1}{2}}}, \quad (9)$$

where $\text{cov}(U_{Mea}, U_{Ref})$ is the covariance of U_{Mea} and U_{Ref} , $\text{var}[U_{Mea}]$ and $\text{var}[U_{Ref}]$ are the variance of U_{Mea} and U_{Ref} , respectively. When no temperature was applied to the FUT, the ACM with ~17 m and ~108 m long DF, and SCM with the arc end were used to calculate the cross-correlation coefficient, i.e., ρ , of the compensated signal along ~108 m FUT, respectively. According to Eq. (6), the spatial resolution could be calculated to 3 mm when a sliding window of $N = 36$ sampling points was used to select the sensing range. To identify small spectral fluctuations, the sliding window with a size of 36, i.e., $N = 36$, could be interpolated by adding 4060 zeros, i.e., $M = 4060$. In this way, the spectral resolution could be improved from $\Delta\nu/N$ to $\Delta\nu/(N \pm M)$, i.e., 34.72 to 0.31 GHz [22, 23]. When the length of DF in the AI was ~17 m, the cross-correlation coefficient obtained by using the ACM was dropped sharply along the FUT, as shown in the green dot in Fig. 6(a). As shown in the

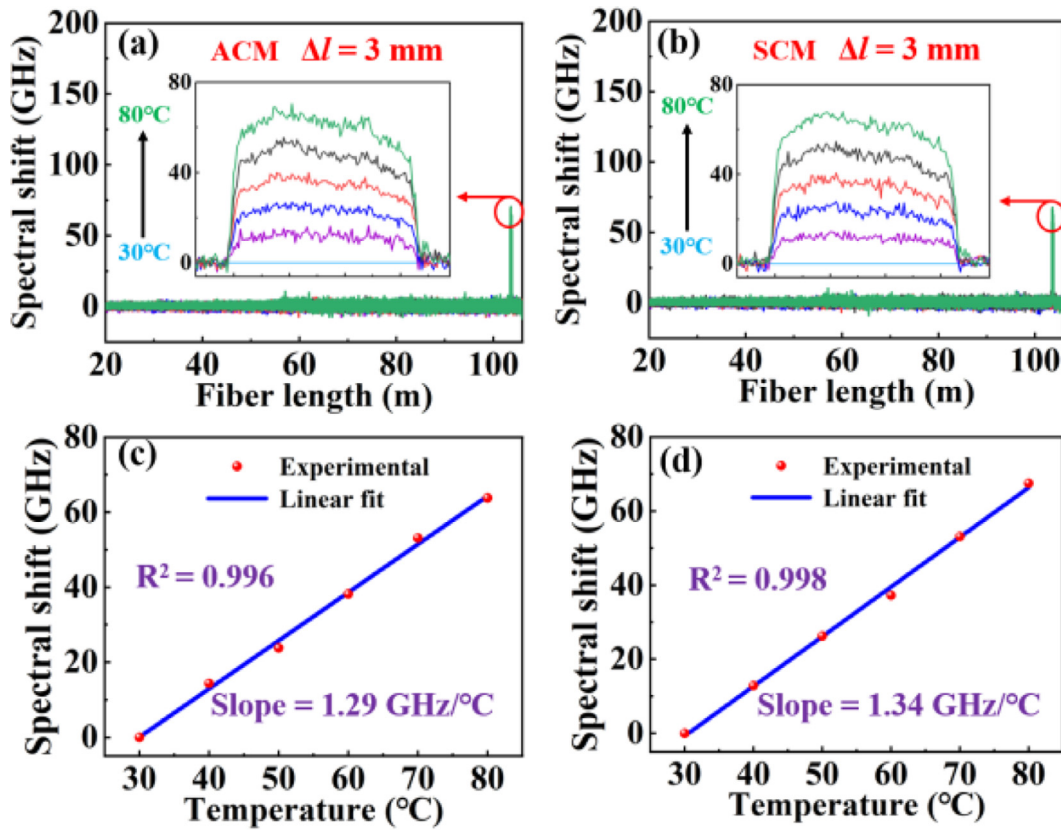


Fig. 7. Obtained spectral shifts of the FUT by using the (a) ACM and (b) SCM, respectively, where the spatial resolution was 3 mm. Note that the temperature was increased from 30 to 80 °C with a step of 10 °C; Obtained spectral shift as a function of temperature for (c) ACM and (d) SCM, respectively. Inset of Figs. (a) and (b): enlarged views of the spectral shifts induced by the temperature increase.

green curve in Fig. 6(b), the spectral shift was also most zero within the distance of 0~40 m, while the spectral shift with obvious error was observed within the distance of 40 ~ 108 m, corresponding to $\theta(t)-\theta(t-\tau_z) \ll \theta(t)-\theta(t-\tau_i)$, and the calculated root mean square error (RMSE) in the range of 0 ~ 108 m was 121.02 GHz. The value of the cross-correlation coefficient calculated by using the ACM with a 108 m DF in the AI was higher than that calculated by using 17 m DF, as shown in the red point in Fig. 6(a). Similarly, the value of the cross-correlation coefficient calculated by using the SCM with the arc end was also kept at a high level along the FUT, as shown in the blue point in Fig. 6(a), indicating that the sensing performance of the proposed system is almost independent of the distance between the arc end of the FUT and the measurement area. The reason for these phenomenon is that both the ACM based on a 108 m DF and SCM based on arc end meet the condition, i.e., $\theta(t)-\theta(t-\tau_z) \geq \theta(t)-\theta(t-\tau_i)$. Moreover, the spectral shifts obtained by the ACM and SCM with 108 m DF exhibited a tiny fluctuation near zero, as shown in the red and blue curve in Fig. 6(b), corresponding to the RMSE of 0.92 and 0.99 GHz, respectively. Therefore, the obtained experimental results were consistent with the above theoretical analysis.

In addition, the temperature sensing performance of the OFDR with AI by using the ACM and single interferometer by using the SCM was also compared. Note that the sweep range and rate were the same as those in Fig. 6, i.e., 10 nm and 80 nm/s. To better illustrate the effectiveness of the proposed method, the temperature furnace was placed near the arc end with the higher phase noise, i.e., 103.47–103.83 m, where the total length of the FUT was ~ 108 m. Note that the length of DF in the conventional OFDR with AI was set to be almost equal to the FUT. The beat signal obtained at the temperature of 30 °C was defined as reference signal, while the beat signals obtained at the temperatures of 40 to 80 °C

were measurement signals. Then the ACM and SCM were employed to compensate the afore-obtained signals, i.e., obtaining compensated reference and measurement signals. The total time for completing a single temperature measurement, including acquisition and signal processing, was about 4 s. As shown in Fig. 7(a) and its enlarged view, large spectral shifts, i.e., up to ~ 68 GHz, were observed in the region with temperature change, while only some tiny spectral shifts probably caused by noise and unstable ambient temperature were observed in the region without temperature change. This indicated that the spectral shift induced by the temperature change of the conventional OFDR with AI was successfully demodulated, when the sensing spatial resolution, i.e., Δl , and spectral resolution were 3 mm ($N = 36$) and 0.31 GHz, respectively. As shown in Fig. 7(c), the temperature sensitivity and linear fitting coefficient of the ACM were 1.29 GHz/°C and 0.996, respectively. Similarly, the spectral shifts could also be successfully obtained by using the SCM with the same spatial resolution and spectral resolution, as shown in the Fig. 7(b) and (d), where the temperature sensitivity and linear fitting coefficient were 1.34 GHz/°C and 0.998, respectively. This indicated that the proposed OFDR with single interferometer could also accurately sense the change of temperature. Therefore, the proposed OFDR with single interferometer could still achieve a high-spatial-resolution of 3 mm for more than 100 m FUT, when the sweep range of the TLS was 10 nm. However, only a spatial resolution of 45 mm was achieved for 50 m FUT, when the sweep range was 20 nm [19].

To illustrate that the proposed OFDR can achieve longer-distance sensing at high-spatial-resolution, the length of FUT was further increased to ~170 m. Compared with Fig. 6(a), the value of the cross-correlation coefficient was decreased when the spatial resolution was 5 mm, as shown in Fig. 8(a). The reason is as follows. On the one hand,

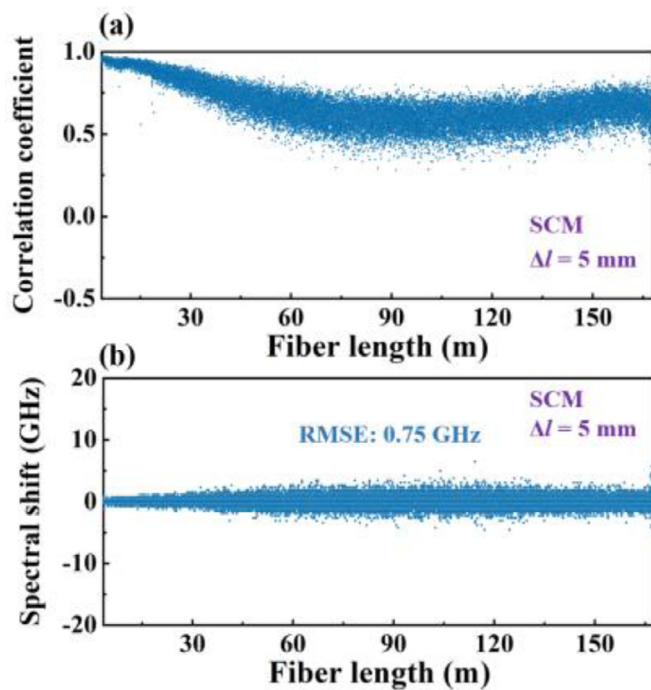


Fig. 8. (a) Cross-correlation coefficient and (b) spectral shift obtained by using SCM while no temperature change was applied to the 170 m long FUT. Note that the spatial resolution, i.e., Δl , was 5 mm.

the phase noise and SNR are deteriorated with the increase of the distance of the FUT [24,25]. On the other hand, the interpolation error is further increased, which is an important reason. As shown in Fig. 8(b), the spectral shift obtained by the SCM could still maintain a tiny fluctuation near zero, where the calculated RMSE was 0.75 GHz.

4. Conclusion

In conclusion, we demonstrated a high-spatial-resolution OFDR with single interferometer based on the SCM. The actual IOF of the TLS was successfully obtained through the arc end of FUT, and the compensated signal with high SNR was obtained by eliminating the phase noise through the SCM. The relative errors of IOFs were relatively tiny, i.e., within 0.006%, at different sweep rates, i.e., 50, 80, 150, and 160 nm/s, respectively. The value of the cross-correlation coefficient calculated by using the SCM was kept at a high level. And the spectral shifts obtained by the ACM and SCM with 108 m DF exhibited a tiny fluctuation near zero, corresponding to the RMSE of 0.92 and 0.99 GHz, respectively. The proposed OFDR achieved the distributed temperature sensing with a high-spatial-resolution of 3 mm without sacrificing measurement performance, where the measured distance of the FUT was ~ 108 m. In addition, the spatial resolution was slightly decreased to 5 mm when the measured distance of the FUT was increased to ~ 170 m, corresponding to the RMSE of spectral shift of 0.72 GHz. Therefore, such an OFDR with simple configuration and good performance has development potential in the field of distributed measurement.

Declaration of Competing Interest

The authors declare that they have no known competing financial interests or personal relationships that could have appeared to influence the work reported in this paper.

CRediT authorship contribution statement

Huajian Zhong: Conceptualization, Methodology, Software, Data curation, Investigation, Writing – original draft. **Cailing Fu:** Supervision, Funding acquisition, Writing – review & editing. **Lijie Wang:** Software. **Bin Du:** Validation. **Pengfei Li:** Investigation. **Yanjie Meng:** Visualization. **Lin Chen:** Formal analysis. **Chao Du:** Formal analysis. **Yiping Wang:** Funding acquisition, Supervision, Project administration.

Data availability

Data will be made available on request.

Acknowledgments

This work was supported by National Natural Science Foundation of China (NSFC) [Grant Nos. 61905155, U1913212]; Natural Science Foundation of Guangdong Province [Grant Nos. 2019B1515120042, 2019A1515011393 and 2021A1515011925]; Science and Technology Innovation Commission of Shenzhen [Grant Nos. JCYJ20200109114020865, JCYJ20200109114201731 and 20200810121618001]; the Shenzhen Key Laboratory of Photonic Devices and Sensing Systems for Internet of Things.

References

- [1] Eickhoff W, Ulrich R. Optical frequency domain reflectometry in single-mode fiber. *Appl Phys Lett* 1981;39(4):693–5.
- [2] Barnoski MK, Jensen SM. Fiber waveguides: a novel technique for investigating attenuation characteristics. *Appl Opt* 1976;15(9):2112–15.
- [3] Peng F, Wu H, Jia X, Rao Y, Wang Z, Peng Z. Ultra-long high-sensitivity Phi-OTDR for high spatial resolution intrusion detection of pipelines. *Opt Express* 2014;22(11):13804–10.
- [4] Wang Z, Zhang L, Wang S, Xue N, Peng F, Fan M, Sun W, Qian X, Rao J, Rao Y. Coherent Φ -OTDR based on I/Q demodulation and homodyne detection. *Opt Express* 2016;24(2):853–8.
- [5] Ding Z, Wang C, Liu K, Jiang J, Yang D, Pan G, Pu Z, Liu T. Distributed optical fiber sensors based on optical frequency domain reflectometry: a review. *Sensors* 2018;18(4):1072–85.
- [6] Feng W, Wang M, Jia H, Xie K, Tu G. High precision phase-OFDR scheme based on fading noise suppression. *J Lightwave Technol* 2022;40(4):900–8.
- [7] Luo M, Liu J, Tang C, Wang X, Lan T, Kan B. 0.5 mm spatial resolution distributed fiber temperature and strain sensor with position-deviation compensation based on OFDR. *Opt Express* 2019;27(24):35823–35289.
- [8] Gui X, Li Z, Fu X, Wang C, Wang H, Wang F, Bao X. Large-scale multiplexing of a FBG array with randomly varied characteristic parameters for distributed sensing. *Opt Lett* 2018;43(21):5259–62.
- [9] Ma G, Zhou H, Li Y, Zhang H, Qin W, Li C, Yan C. High-resolution temperature distribution measurement of GIL spacer based on OFDR and ultraweak FBGs. *IEEE Trans Instrum Meas* 2020;69(6):3866–73.
- [10] Li P, Fu C, Du B, He J, Zhong H, Du C, Wang L, Wang Y. High-spatial-resolution strain sensor based on distance compensation and image wavelet denoising method in OFDR. *J Lightwave Technol* 2021;39(19):6334–9.
- [11] Feng K, Cui J, Jiang D, Dang H, Jin Y, Sun X, Niu Y, Tan J. Improvement of the strain measurable range of an OFDR based on local similar characteristics of a Rayleigh scattering spectrum. *Opt Lett* 2018;43(14):3293–6.
- [12] Meng Y, Fu C, Du C, Chen L, Zhong H, Li P, Xu B, Du B, He J, Wang Y. Shape sensing using two outer cores of multicore fiber and optical frequency domain reflectometer. *J Lightwave Technol* 2021;39(20):6624–30.
- [13] Du Y, Jothibas S, Zhuang Y, Zhu C, Huang J. Rayleigh backscattering based macrobending single mode fiber for distributed refractive index sensing. *Sens Actuators B Chem* 2017;248:346–50.
- [14] Moore ED, McLeod RR. Correction of sampling errors due to laser tuning rate fluctuations in swept-wavelength interferometry. *Opt Express* 2008;16(17):13139–49.
- [15] Feng B, Liu K, Liu T, Jiang J, Du Y. Improving OFDR spatial resolution by reducing external clock sampling error. *Opt Commun* 2016;363:74–9.
- [16] Ahn TJ, Lee JY, Kim DY. Suppression of nonlinear frequency sweep in an optical frequency-domain reflectometer by use of Hilbert transformation. *Appl Opt* 2005;44(35):7630–4.
- [17] Yao Z, Mauldin T, Xu Z, Hefferman G, Wei T. An integrated OFDR system using combined swept-laser linearization and phase error compensation. *IEEE Trans Instrum Meas* 2021;70:1–8.
- [18] Sagiv OY, Arbel D, Eyal A. Correcting for spatial-resolution degradation mechanisms in OFDR via inline auxiliary points. *Opt Express* 2012;20:27465 no.pp.
- [19] Badar M, Lu P, Buric M, Ohodnicki P. Integrated auxiliary interferometer for self-correction of nonlinear tuning in optical frequency domain reflectometry. *J Lightwave Technol* 2020;38(21):6097–103.

- [20] Yin G, Jiang R, Zhu T. In-fiber auxiliary interferometer to compensate laser nonlinear tuning in simplified OFDR. *J Lightwave Technol* 2022;40(3):837–43.
- [21] Wang B, Fan X, Wang S, He Z. Phase-dispersion spectroscopy with high spectral resolution using a wideband ultra-linearly swept optical source. *J Lightwave Technol* 2019;37(13):3127–37.
- [22] Cui J, Zhao S, Yang D, Ding Z. Investigation of the interpolation method to improve the distributed strain measurement accuracy in optical frequency domain reflectometry systems. *Appl Opt* 2018;57(6):1424–31.
- [23] Wang C, et al. High sensitivity distributed static strain sensing based on differential relative phase in optical frequency domain reflectometry. *J Lightwave Technol* 2020;38(20):5825–36.
- [24] Venkatesh S, Sorin WV. Phase noise considerations in coherent optical FMCW reflectometry. *J Lightwave Technol* 1993;11(10):1694–700 Oct..
- [25] Zhang Z, Fan X, Wu M, He Z. Phase-noise-compensated OFDR realized using hardware-adaptive algorithm for real-time processing. *J Lightwave Technol* 2019;37(11):2634–40.